Chemical Science

Accepted Manuscript

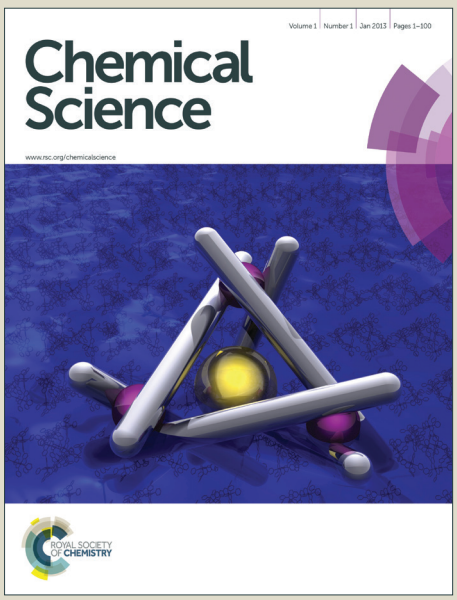

ROYAL SOCIETY OF CHEMISTRY

www.rsc.org/chemicalscience

Journal Name

RSCPublishing

ARTICLE

Electron-Accepting Phthalocyanine-Pyrene Conjugates: Towards Liquid Phase Exfoliation of Graphite and Photoactive Nanohybrid Formation with Graphene

Cite this: DOI: 10.1039/xoxxoooooox

Received ooth January 2012,
Accepted ooth January 2012

DOI: 10.1039/xoxxoooooox

www.rsc.org/

Alexandra Roth,[a] Maria-Eleni Ragoussi,[b] Leonie Wibmer,[a] Georgios Katsukis,[a] Gema de la Torre,[b*] Tomás Torres,[b,c*] Dirk M. Guldi[a*]

Herein, we describe the synthesis of a zinc(II) alkylsulfonylphthalocyanine-pyrene conjugate, its assembly with highly exfoliated graphite, and the investigation of the photophysical properties of the resulting nanohybrid. The presence of the pyrene unit in the conjugate is decisive in terms of non-covalently immobilizing the electron accepting phthalocyanines onto the basal plane of highly exfoliated graphite. As a matter of fact, strong interactions dominate the electronic properties of the nanohybrid in both the ground and excited states. For example, femtosecond pump probe experiments assist in corroborating an ultrafast charge separation, that is, the generation of the one-electron reduced radical anion of the phthalocyanine and one-electron oxidized graphene after irradiation at 387 nm, followed by slow charge recombination.

Introduction

Single layer graphene features many interesting properties like high strength and stiffness combined with excellent thermal and electrical conductivity.[1] Thus, graphene bears the potential to be used in emerging applications such as ultrafast transistors,[2] strong and tough composites,[3] touch screens,[4] and energy conversion systems.[5] In the context of solar energy conversion schemes, highly efficient solar cells based on graphene have been envisaged, since it was demonstrated that this material converts light of any given wavelength into photocurrents.[6] However, the practical use of graphene is limited due to the difficulty of its production in high quality, on a large scale, and at low cost in a reproducible manner.

Notably, the micromechanical cleavage of graphite is a very successful approach to produce high-quality single layer graphene.[1] It features, however, huge drawbacks during up-scaling. Beside the latter, thermal chemical vapor deposition (CVD),[7,8] epitaxial growth on SiC substrates,[9] chemical synthesis,[10,11] as well as chemical exfoliation[12,13] are commonly used to produce graphene. Among them, wet chemical exfoliation of bulk graphite constitutes by far the most intriguing approach to mass produce high-quality graphene monolayers on an industrial scale and at low costs.

Liquid-phase exfoliation of graphite is performed by sonication of graphite powder in either a variety of organic solvents or aqueous solutions containing different surfactants. Here, ultrasonication provides the energy needed to overcome the π-π stacking between individual graphene layers and, in turn, to cleave such interactions.[14] Next to organic solvents, planar, aromatic building blocks such as porphyrins,[15] pyrene derivatives,[16-19] perylene diimides,[20] conjugated polymers,[21,22] etc, which all reveal strong affinities towards the basal plane of graphene in the form of π-π stacking, assist in the exfoliation of graphite and in the stabilization of the exfoliated material. An additional asset of non-covalent interactions between aromatic molecules and graphene is that it provides the means to add light harvesting and charge transfer features to the latter. At the same time, the lattice structure of graphene, which reveals most of its intrinsic electronic properties, remains intact. As a matter of fact, the resulting nanohybrid materials bear great potential for solar energy conversion applications,[23,24] especially when photo- and redoxactive chromophores, such as porphyrins or phthalocyanines,[25,26] are involved in the graphite exfoliation and graphene stabilization.

In recent work, we successfully demonstrated the exfoliation of graphite in solution by taking advantage of non-covalent interactions with porphycenes,[27] phthalocyanines,[28] porphyrins,[29,30] etc, and realized single layer / bilayer nano-graphene charge transfer nanohybrids. Spectroscopic as well as kinetic evidences were established not only for ground-state interactions, but also for interactions in the excited state. In particular, nanohybrids formed from exfoliated graphene and poly-*para*-phenylenevinylene oligomers containing lateral

electron donating phthalocyanines featured ultrafast charge separation evolving from photoexcited Zn(II) phthalocyanine to graphene.[28] A similar trend was confirmed in a covalent graphene nanoconjugate carrying electron donating phthalocyanines.[31]

Notably, tailor-made electron accepting phthalocyanines are realized by placing suitable substituents at their periphery. For instance, alkylsulfonyl chains are appropriate to reduce the HOMOs and LUMOs of the aromatic core. Following this general approach, electron-accepting phthalocyanines have been covalently linked to the basal plane of exfoliated graphene. In the resulting nanoconjugate, electron transfer evolves from the graphene layers to the photoexcited phthalocyanine.[32]

As aforementioned, pyrene and its derivatives display a strong affinity towards sp^2-nanocarbon networks.[16,33] For instance, functionalization of phthalocyanines with pyrene addenda has shown to assist in the non-covalent immobilization of chromophores onto carbon nanotubes, in general, and single wall carbon nanotubes, in particular[34,35] Zn(II) phthalocyanines bearing four pyrene units form non-covalent ensembles with few-layer graphene, the nanoconjugate proving ultrafast charge transfer from the photoexcited chromophore to the acceptor exfoliated graphite.[36]

In the current work, we present a novel electron-accepting phthalocyanine-pyrene conjugate **2** that stabilizes single layer graphene during the ultrasonication of graphite by virtue of electronic interactions. Alkylsulfonyl-substituted phthalocyanines, which lack the pyrene addenda, were also found to form nanohybrids with exfoliated graphene. This process is, however, less efficient in the latter case than in the earlier. By means of full-fledged photophysical investigations, we corroborated that the electronic interactions in the ground and excited state in the nanohybrids are indeed very strong. As such, after photoexcitation of the nanoconjugate, an electron transfer takes place from the basal plane of graphene to the immobilized electron accepting phthalocyanines.

Results and Discussion

Synthesis and spectroscopic characterization of phthalocyanines

Phthalocyanine-pyrene conjugate **2** was prepared in one step starting from the unsymmetrically substituted, alkylsulfonyl-Pc-hydroxyl derivative **1**, recently described by us – Scheme 1.[32] The esterification reaction between Pc and 1-pyrene butyric acid, in the presence of EDC and DMAP proceeded smoothly and afforded the desired conjugate in 65% yield.

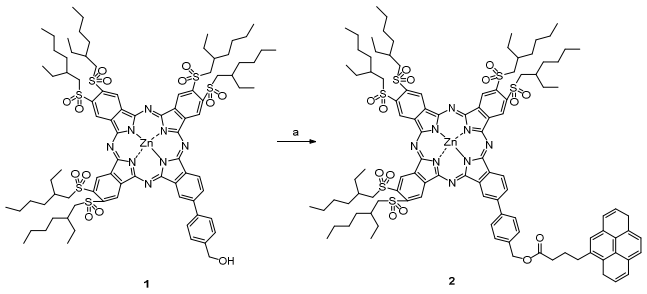

Scheme 1. Synthesis of phthalocyanine-pyrene **2**. Reagents and conditions: a) 1-pyrene butyric acid, EDC, DMAP, 0°C to room temperature, 48 h.

Initially, the ground state characteristics of phthalocyanine-pyrene **2** and its precursor, lacking the pyrene addenda, that is, **1** (Scheme 1), were investigated. In this context, steady-state absorption spectroscopic measurements were performed. Both spectra revealed the typical phthalocyanine Q-band absorptions at 676 and 711 nm and the Soret-band absorptions at 375 nm for **1** and **2** – see Figure 1. The split of the Q-band is caused by the unsymmetrical substitution, which lowers the symmetry of the electronic structure. The spectrum of **2** revealed also the characteristic pyrene features at 330 and 345 nm.

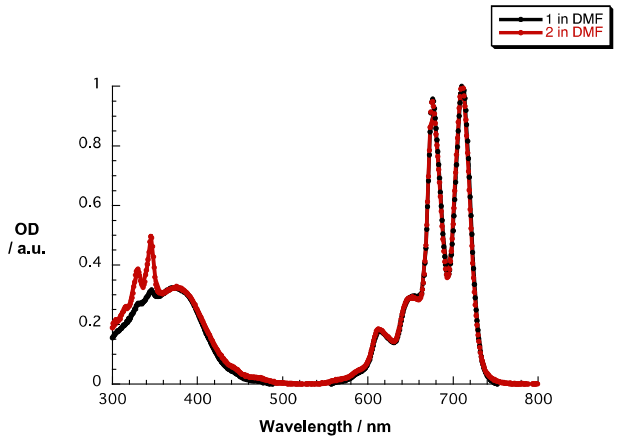

Figure 1. Normalized absorption spectra of **1** (black spectrum) and **2** (red spectrum) in DMF.

In addition, square wave voltammetry and cyclic voltammetry measurements were carried out with **1** and **2** in *o*-dichlorobenzene containing 0.05 M tetra-*tert*-butyl ammonium hexafluorophosphate as supporting electrolyte with a glassy carbon working electrode, a platin wire as counter electrode, and a silver wire as pseudo-reference electrode. If not otherwise stated, the redox potentials are given *vs*. ferrocene/ferrocenium. For **2**, one reversible oxidation was noted at 0.58 V followed by two reversible reductions at -0.97 and -1.19 V. The redox potentials for **1** correlate with an oxidation at 0.61 V and a reduction at -1.10 V. Based on these results, spectroelectrochemical measurements were performed in acetonitrile:toluene 1:4 (v/v). Here, a platinum net was employed as working electrode. Upon applying a voltage of -0.7 V *vs*. Ag-wire, **2** showed new absorption maxima at 485,

582, 760, 920, and 960 nm – Figure 2. Under these reductive conditions, the newly developing features can be assigned to the one-electron reduced species. Notably, the reversibility was confirmed by applying several electrochemical cycles between -0.7 and 0.1 V vs. Ag-wire. Consistent with the spectral changes seen upon reducing phthalocyanine-pyrene **2**, experiments with **1** were essentially identical – Figure S1. It can, thus, be concluded that the presence of pyrene has no significant influence on the redox behavior of the phthalocyanine.

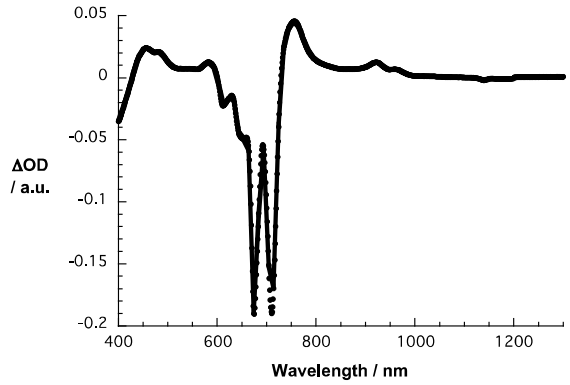

Figure 2. Differential absorption spectrum obtained upon electrochemical reduction of **2** in acetonitrile:toluene 1:4 (v/v) with 0.1 M $TBAPF_6$ and an applied potential of -0.7 V vs. Ag-wire.

Following the ground state characterization, the excited state features of **1** and **2** were probed. Among them, fluorescence spectroscopic measurements stood at the forefront. In the corresponding fluorescence spectra – Figure 3 – a strong maximum at 723 nm, a weak maximum at 797 nm and a weak shoulder at 755 nm were discernable.

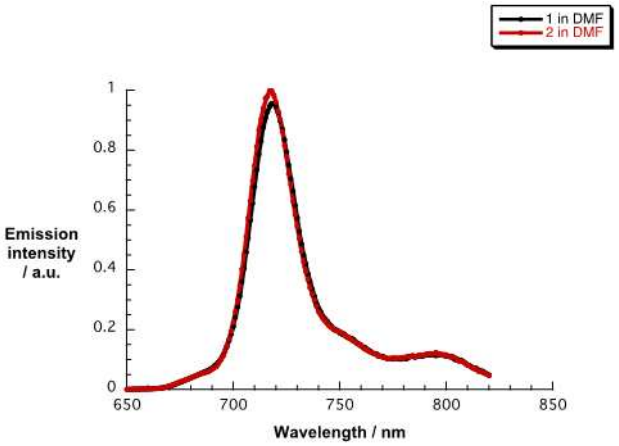

Figure 3. Normalized emission spectra of **1** (red spectrum) and **2** (black spectrum) in DMF upon excitation at 630 nm.

Using tetra-*tert*-butyl zinc (II) phthalocyanine as reference, the fluorescence quantum yields in a toluene:pyridine (100:1 v/v) mixture were determined as 21.8 and 23.1% for **1** and **2**, respectively. Important is the fact that the excitation spectra of **1** and **2** resemble the absorption spectra and, thus, confirm the non-aggregated status of **1** and **2**. Turning to time resolved spectroscopy, the fluorescence lifetimes were determined by means of time-correlated-single-photon-counting (TCSPC) measurements. Figure S2 documents that following excitation at 647 nm of **1** and **2** under argon in DMF led to fluorescence decays that were best fit by lifetimes of 2.05 and 2.00 ns, respectively. Complementary femtosecond transient absorption measurements were performed in DMF with an excitation wavelength of 387 nm. These measurements as shown in Figure S3, revealed transient absorption maxima at 524 and at 849 nm for **1** in DMF corresponding to singlet-singlet transitions. Additional ground state bleaching in the range between 600 and 750 nm with minima at 679 and 719 nm complement the singlet excited state features. The singlet excited state characteristics of **1** transform to those of the corresponding triplet excited state via intersystem crossing within a timescale of 2.1 ns. The main features of the latter are maxima at 788 and at 465 nm. Next to **1**, also **2** was probed by femtosecond transient absorption spectroscopy – see Figure 4.

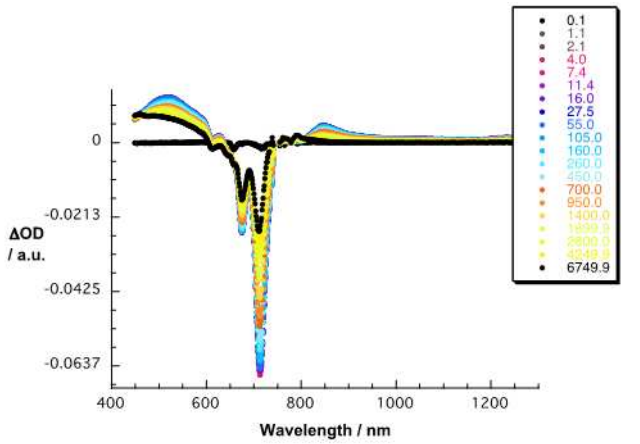

Figure 4. Differential absorption spectra (visible and near-infrared) obtained upon femtosecond pump probe experiments (387 nm) of **2** in DMF with time delays between 0.1 and 6749.9 ps at room temperature – for time delays see figure legend.

Here, the singlet excited state of **2** in DMF is characterized by transient maxima at 517 and 850 nm. Furthermore, the spectra reveal a ground state bleaching in the range from 650 to 750 nm with minima at 685 and 708 nm. As in the case of **1**, the triplet excited state of **2** is formed by intersystem crossing within 2.0 ns. The maxima, which relate to the triplet excited state and whose lifetime exceeds the time range of the experimental setup, evolve at 463 and 788 nm.

Synthesis and spectroscopic characterization of nano-hybrids.

The preparation of the desired hybrid systems, that is, either **1** / nanographene or **2** / nanographene, was carried out by

exfoliation of graphite *via* ultrasonic treatment in the presence of **1** and **2** in DMF. An efficient procedure consisted in adding graphite to a 1 x 10^{-5} M solution of either **1** or **2** in DMF and ultrasonicating the mixtures for 45 min. The resulting dispersions were then centrifuged for 15 min at 500 rpm. Then, the supernatant was extracted and used for further enrichment cycles, that is, the addition of graphite, ultrasonication and centrifugation under the same conditions. These enrichment/exfoliation steps were subsequently repeated up to six times. The stability of all the dispersions was carefully tested by steady-state absorption spectroscopy before and after ultrasonication to monitor and identify any resulting spectral changes, as shown below.

Turning to the characterization of **1** / nanographene and **2** / nanographene, we first proceeded to determine the single-, bi-, few-, or multilayer character of the exfoliated graphene after six enrichment cycles. Raman measurements with 532 nm laser excitation were performed. In particular, a Raman map of **2** / nanographene dropcasted onto a Si/SiO_2 wafer was established, and 170 spectra were evaluated. The spectra featured the typical Raman bands for graphene systems, that is, the D-band centered at 1347 cm^{-1} as well as the G- and 2D-bands at 1581 and 2692 cm^{-1}, respectively. Please note that such Raman mapping facilitates the statistical evaluation concerning the 2D/G ratios of, for example, **2** / nanographene – Figure 5. For **2** / nanographene, the distribution was best fit with a log-normal fitting function and centers at a 2D/G ratio of 0.93. The intensity ratio of few- to multilayer graphene is - 0.7 or less.[32] Consequently, the data reveal a distribution of 33 % multilayer graphene / bulk graphite character and of about 67 % single layer / few layer / turbostratic graphene character. Furthermore, the spectra that give rise to 2D/G ratios in excess of 1.0 were closely examined in terms of the FWHM of their 2D bands. 5 % of these spectra were best fit with a single Lorentzian featuring FWHM of about 37 cm^{-1}. From the latter, we derive that 95 % have few layer / turbostratic graphene character, while 5 % are real single layer graphene. Please note that the samples are prepared by drop-casting a dispersion of the nanohybrid onto the corresponding Si/SiO_2 wafers and, as such, more single layer graphene are unlikely to be found. The high amount of turbostratic graphene is, nevertheless, indicative for a successful exfoliation. As such, further optimization of the deposition onto the Si/SiO_2 wafers is expected to result in more single layer graphene flakes. The Raman maps of **1** / nanographene, which were measured under the same experimental conditions, led to slightly lower 2D/G ratios with log-normal fitting functions that center at 0.79 – Figure S4. Here, 42 % represent few- to multilayer graphene / bulk graphite. From this, it can be concluded that, as previously established, the presence of the pyrene addenda in the phthalocyanine improves the exfoliation/inmobilization process.

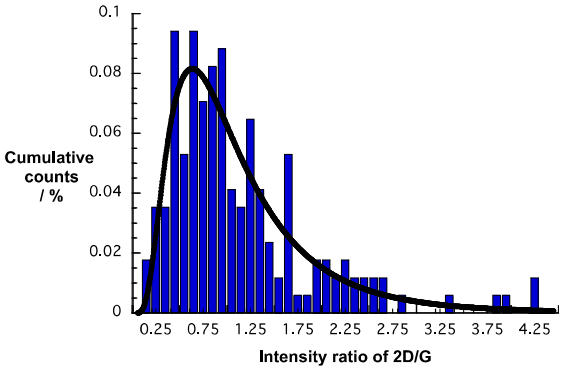

Figure 5. Histogram resulting from the Raman mapping of **2** / nanographene showing relative counts vs. I(2D) / I(G) ratio and the corresponding log-normal distribution. The sample was drop casted from a DMF dispersion onto silicon oxide wafer and was excited at 532 nm.

In addition to Raman investigations, AFM was used to shed light onto the lateral dimensions and the thickness of flakes obtained for **2** / nanographene. From AFM image analyses we derive, next to few layer graphene, and bulk graphite, also flakes with thicknesses of up to 1 nm – Figure 6 – which is ascribed to single layer graphene.[37]

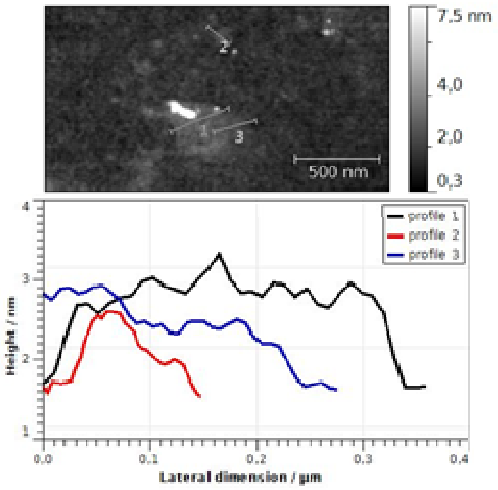

Figure 6. Upper part – tapping mode AFM image of **2** / nanographene drop casted on a SiO_2 surface. Lower part – height profiles at position 1, 2, and 3.

From the measured height profiles we infer that most of the flakes have turbostratic character. This finding is in sound agreement with the results gathered in the Raman measurements. Furthermore, TEM images of **2** / nanographene flakes were taken to corroborate their sizes – Figure 7. The images prompt to flakes with a mean side lengths of up to 200 nm. They also show that the flakes were unruffled and the edges were mainly observed to be multiples of 30°. Edge angles like 60 and 120° indicate same chiralities between two adjacent edges, whereas 30, 90, and 150° are observable when different

chiralities converge.[38] Overall, they confirm the results stemming from AFM and Raman investigations. A representative TEM image of **1** / nanographene is shown in Figure S5.

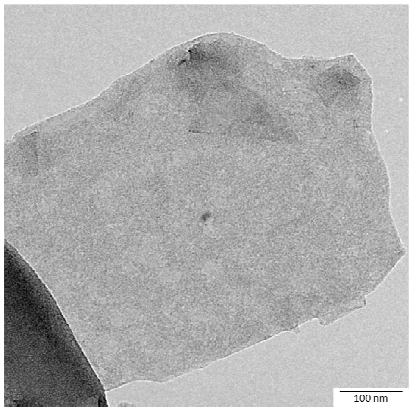

Figure 7. TEM image of **2** / nanographene drop casted on a lacey carbon grid.

Relative to the absorption spectrum of **2**, our enrichment approach led to new absorption features in the spectra recorded in steady-state absorption spectroscopic measurements – Figure 8. On one hand, graphene that is present within the dispersions contributes to the overall increase in optical density, especially in the blue region of the spectra. On the other hand, new Q-band absorptions around 750 nm, markedly red-shifted relative to what is seen for **2**, attest to phthalocyanines that interact strongly with the basal plane of graphene. In line with the aforementioned, fluorescence spectroscopy gave rise to a gradual quenching of the phthalocyanine fluorescence throughout the preparation of **2** / nanographene dispersions. Notably, the fluorescence reveals a quantitative quenching after the 4th enrichment step - see Figure 8. Figure S6 shows the absorption spectra of **1** and of **1** / nanographene after the enrichment process.

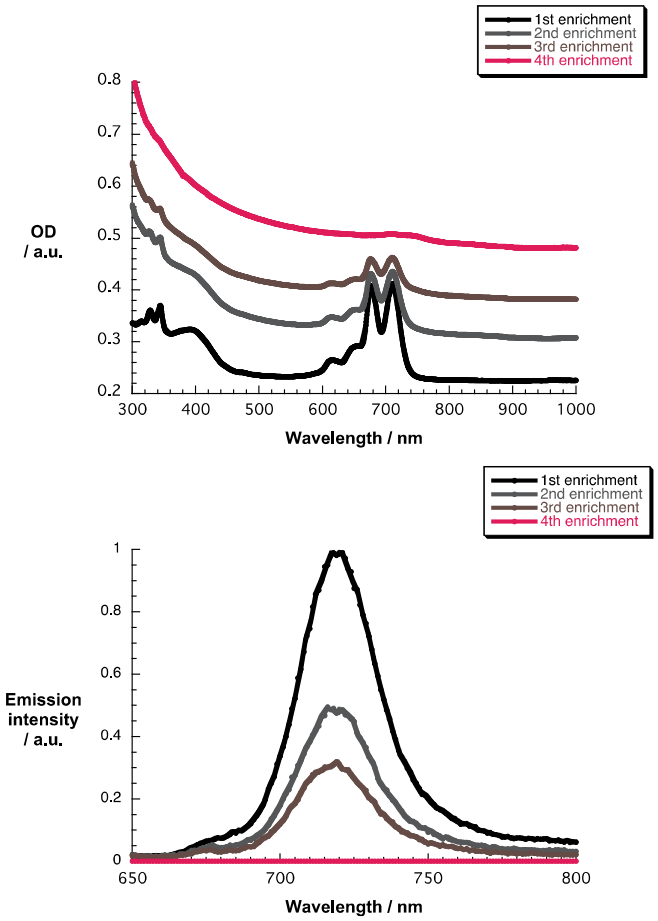

Figure 8. Upper part – absorption spectra of **2** / nanographene in DMF following the 1st to 4th exfoliation/enrichment steps. Lower part – fluorescence spectra of **2** / nanographene in DMF following the 1st to 4th exfoliation/enrichment steps

Turning to time resolved measurements, femtosecond transient absorption spectroscopy was utilized to probe **1** / nanographene and **2** / nanographene systems. In the case of **1** / nanographene, differential absorption spectra ground state bleaching of **1** as well as very weak singlet features are discernable. In addition, the triplet excited state features are noted throughout the visible part of the spectra, which are rationalized in terms of free and non-immobilized phthalocyanine. In fact, the lack of interactions lead to singlet excited lifetimes similar to that found for **1** as shown in Figure S7. In the case of **2** / nanographene system the formation of new transient species are seen (Figure 9). For the latter, maxima at 485, 582, and 760 nm, as well as minima at 460 and 640 nm are in sound agreement with the fingerprints of one-electron reduced phthalocyanine – vide supra. In the near infrared region, the weaker 920 and 960 nm features of the reduced phthalocyanine are, however, masked by the strong phonon related bleaching of graphene. From a mono-exponential fit at, for example, 1100 nm, we determined the lifetime of the graphene bleaching as 0.67 +/- 0.5 ps in both cases. Importantly, new features evolving during the transient decay, which include broad maxima at 950 and 1070 nm, indicate new holes in the valence band of graphene

due to electron transfer from graphene to the phthalocyanines. Figure 9 shows the corresponding time-absorption profile for **2** / nanographene in DMF at 760 nm from which charge separation and charge recombination dynamics of 0.40 +/- 0.5 and 320 +/- 100 ps were derived. The time-absorption profile for **1** / nanographene in DMF at 760 nm led to a slightly faster charge separation of 0.44 +/- 0.5 ps and also a faster charge recombination of 183.8 +/- 46.8 ps – Figure S8. Important is the fact that the phonon-related bleaching of graphene/graphite in the range between 820 and 1300 nm seen for **1** / nanographene and **2** / nanographene has – in reference experiments – nearly the same intensity and, in turn, indicates that approximately the same amount of graphene/graphite is suspended.

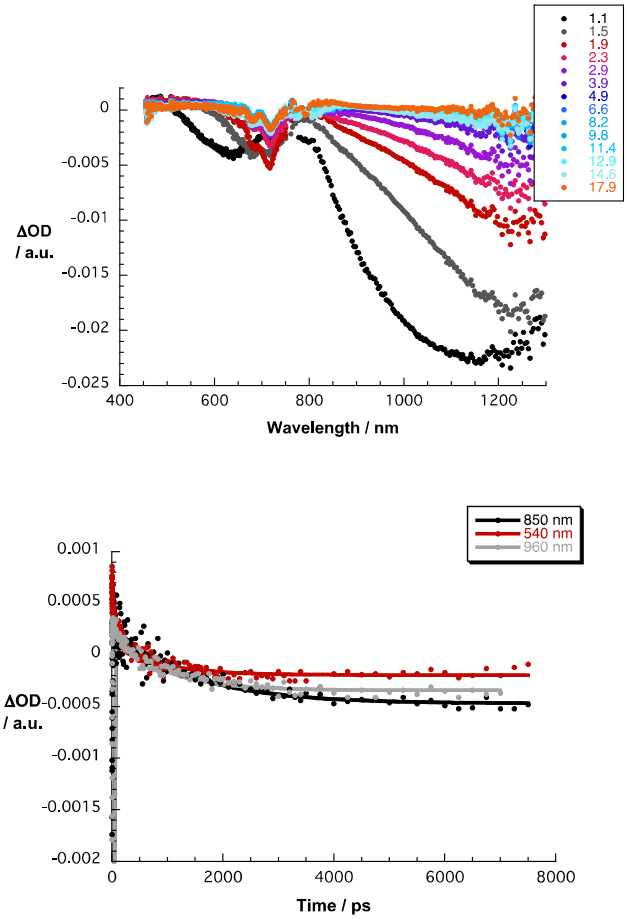

Figure 9. Upper part – differential absorption spectra (visible and near-infrared) obtained upon femtosecond pump probe experiments (387 nm) of **2** / nanographene in DMF with time delays between 1.1 and 17.9 ps at room temperature – for time delays see figure legend. Lower part – time absorption profiles of the spectra shown in the upper part at 540, 850 and 960 nm monitoring the charge transfer.

Conclusions

To sum up, **1** as well as **2** feature lower reduction and higher oxidation potentials compared to unsubstituted phthalocyanines or those substituted with electron-donating groups. The successful preparation of **1** / nanographene and **2** / nanographene, which was based on the enrichment technique, in which graphite was added to concentrated solutions of **1** and **2** followed by ultrasonication, centrifugation and supernatant extraction, was demonstrated by Raman measurements, together with ground-state spectroscopy, and AFM and TEM microscopies. The corresponding spectra corroborate the successful exfoliation of graphite. Notably, pyrene exerts a strong influence on the stabilization of graphene sheets formed upon ultrasonication induced exfoliation. Furthermore after preparing **1** / nanographene and **2** / nanographene dispersions, steady-state absorption spectra gave rise to new features that prompt to strong electronic coupling between the phthalocyanines and the basal plane of graphene. Transient absorption spectroscopic measurements corroborate that this electronic coupling is the inception for a photoinduced electron transfer from graphene to the phthalocyanines, both in **1** / nanographene and in **2** / nanographene. Importantly, the formation of one-electron reduced phthalocyanines upon irradiation of the nanohybrids is supported by spectroelectrochemical experiments.

Acknowledgements

Financial support is acknowledged from the Spanish MEC, MICINN, MINECO (CTQ2011-24187/BQU, PIB2010US-00652, PRI-PIBUS-2011-1128), and the Deutsche Forschungsgemeinshaft (SFB 583 and FCI).

Notes and references

[a] Department of Chemistry and Pharmacy and Interdisciplinary Center for Molecular Materials (ICMM) Friedrich-Alexander-Universität Erlangen-Nürnberg 91058 Erlangen (Germany).
[b] Departamento de Química Orgánica, Universidad Autónoma de Madrid Cantoblanco, 28049-Madrid, Spain.
[c] IMDEA-Nanociencia, c/ Faraday 9, Campus de Cantoblanco, 28049-Madrid, Spain.
*Corresponding author: gema.delatorre@uam.es
*Corresponding author: tomas.torres@uam.es
*Coressponding author: dirk.guldi@fau.de

Electronic Supplementary Information (ESI) available: [details of any supplementary information available should be included here]. See DOI: 10.1039/b000000x/

1. K. S. Novoselov, A. K. Geim, S. V. Morozov, D. Jiang, Y. Zhang, S. V. Dubonos, I. V. Grigorieva and A. A. Firsov, *Science*, 2004, **306**, 666-669.
2. Y.-M. Lin, C. Dimitrakopoulos, K. A. Jenkins, D. B. Farmer, H.-Y. Chiu, A. Grill and P. Avouris, *Science*, 2010, **327**, 662.
3. R. J. Young, I. A. Kinloch, L. Gong and K. S. Novoselov, *Compos. Sci. Technol.*, 2012, **72**, 1459-1476.
4. S. Bae, H. Kim, Y. Lee, X. Xu, J.-S. Park, Y. Zheng, J. Balakrishnan, T. Lei, H. Ri Kim, Y. I. Song, Y.-J. Kim, K. S. Kim, B. Ozyilmaz, J.-H. Ahn, B. H. Hong and S. Iijima, *Nature Nanotech.*, 2010, **5**, 574-578.
5. Y. Cheng, H. Zhang, C. V. Varanasi and J. Liu, *Energy Environ. Sci.*, 2013, **6**, 3314-3321.

6. M. Bernardi, J. Lohrman, P. V. Kumar, A. Kirkeminde, N. Ferralis, J. C. Grossman and S. Ren, *ACS Nano*, 2012, **6**, 8896-8903.
7. A. Reina, X. Jia, J. Ho, D. Nezich, H. Son, V. Bulovic, M. S. Dresselhaus and J. Kong, *Nano Lett.*, 2009, **9**, 30-35.
8. X. Li, W. Cai, J. An, S. Kim, J. Nah, D. Yang, R. Piner, A. Velamakanni, I. Jung, E. Tutuc, S. K. Banerjee, L. Colombo and R. S. Ruoff, *Science*, 2009, **324**, 1312-1314.
9. C. Berger, Z. Song, X. Li, X. Wu, N. Brown, C. Naud, D. Mayou, T. Li, J. Hass, A. N. Marchenkov, E. H. Conrad, P. N. First and W. A. de Heer, *Science*, 2006, **312**, 1191-1196.
10. X. Yang, X. Dou, A. Rouhanipour, L. Zhi, H. J. Rader and K. Mullen, *J. Am. Chem. Soc*, 2008, **130**, 4216-4217.
11. L. Chen, Y. Hernandez, X. Feng and K. Mullen, *Angew. Chem. Int. Ed.*, 2012, **51**, 7640-7654.
12. Y. Hernandez, V. Nicolosi, M. Lotya, F. M. Blighe, Z. Sun, S. De, I. T. McGovern, B. Holland, M. Byrne, Y. K. Gun'Ko, J. J. Boland, P. Niraj, G. Duesberg, S. Krishnamurthy, R. Goodhue, J. Hutchison, V. Scardaci, A. C. Ferrari and J. N. Coleman, *Nature Nanotechnol.*, 2008, **3**, 563-568.
13. D. Li, M. B. Muller, S. Gilje, R. B. Kaner and G. G. Wallace, *Nature Nanotechnol*, 2008, **3**, 101-105.
14. G. Cravotto and P. Cintas, *Chem. - Eur. J.*, 2010, **16**, 5246-5259.
15. J. Geng, B.-S. Kong, S. B. Yang and H.-T. Jung, *Chem. Commun.*, 2010, **46**, 5091-5093.
16. Q. Su, S. Pang, V. Alijani, C. Li, X. Feng and K. Müllen, *Adv. Mater.*, 2009, **21**, 3191-3195.
17. X. An, T. Simmons, R. Shah, C. Wolfe, K. M. Lewis, M. Washington, S. K. Nayak, S. Talapatra and S. Kar, *Nano Lett.*, 2010, **10**, 4295-4301.
18. S. Sampath, A. N. Basuray, K. J. Hartlieb, T. Aytun, S. I. Stupp and J. F. Stoddart, *Adv. Mater.*, 2013, **25**, 2740-2745.
19. F. Zhang, X. Chen, R. A. Boulos, F. M. Yasin, H. Lu, C. Raston and H. Zhang, *Chem. Commun.*, 2013, **49**, 4845-4847.
20. N. V. Kozhemyakina, J. M. Englert, G. Yang, E. Spiecker, C. D. Schmidt, F. Hauke and A. Hirsch, *Adv. Mater.*, 2010, **22**, 5483-5487.
21. Z. Liu, Q. Liu, Y. Huang, Y. Ma, S. Yin, X. Zhang, W. Sun and Y. Chen, *Adv. Mater.*, 2008, **20**, 3924-3930.
22. M. Castelain, H. J. Salavagione, R. Gomez and J. L. Segura, *Chem. Commun.*, 2011, **47**, 7677-7679.
23. K. Dirian, M. A. Herranz, G. Katsukis, J. Malig, L. Rodriguez-Perez, C. Romero-Nieto, V. Strauss, N. Martin and D. M. Guldi, *Chem. Sci.*, 2013, **4**, 4335-4353.
24. J. Malig, N. Jux and D. M. Guldi, *Acc. Chem. Res.*, 2013, **46**, 53-64.
25. G. de la Torre, C. G. Claessens and T. Torres, *Chem. Commun.*, 2007, 2000-2015.
26. G. Bottari, G. de la Torre, D. M. Guldi and T. Torres, *Chem. Rev.*, 2010, **110**, 6768-6816.
27. R. D. Costa, J. Malig, W. Brenner, N. Jux and D. M. Guldi, *Adv. Mater.*, 2013, **25**, 2600-2605.
28. J. Malig, N. Jux, D. Kiessling, J.-J. Cid, P. Vázquez, T. Torres and D. M. Guldi, *Angew. Chem. Int. Ed.*, 2011, **50**, 3561-3565.
29. J. Malig, A. W. Stephenson, P. Wagner, G. G. Wallace, D. L. Officer and D. M. Guldi, *Chem. Commun.*, 2012, **48**, 8745-8747.
30. D. Kiessling, R. D. Costa, G. Katsukis, J. Malig, F. Lodermeyer, S. Feihl, A. Roth, L. Wibmer, M. Kehrer, M. Volland, P. Wagner, G. G. Wallace, D. L. Officer and D. M. Guldi, *Chem. Sci.*, 2013, **4**, 3085-3098.
31. M. E. Ragoussi, J. Malig, G. Katsukis, B. Butz, E. Spiecker, G. de la Torre, T. Torres and D. M. Guldi, *Angew. Chem. Int. Ed.*, 2012, **51**, 6421-6425.
32. M.-E. Ragoussi, G. Katsukis, A. Roth, J. Malig, G. de la Torre, D. M. Guldi and T. Torres, *J. Am. Chem. Soc.*, 2014, DOI: 10.1021/ja411830x.
33. J. A. Mann, J. Rodríguez-López, H. D. Abruña and W. R. Dichtel, *J. Am. Chem. Soc.*, 2011, **133**, 17614-17617.
34. J. Bartelmess, B. Ballesteros, G. de la Torre, D. Kiessling, S. Campidelli, M. Prato, T. Torres and D. M. Guldi, *J. Am. Chem. Soc.*, 2010, **132**, 16202-16211.
35. M. Ince, J. Bartelmess, D. Kiessling, K. Dirian, M. V. Martínez-Díaz, T. Torres and D. M. Guldi, *Chem. Sci.*, 2012, **3**, 1472.
36. C. B. K. C, S. K. Das, K. Ohkubo, S. Fukuzumi and F. D'Souza, *Chem. Commun.*, 2012, **48**, 11859-11861.
37. Q. H. Wang, C.-J. Shih, G. L. C. Paulus and M. S. Strano, *J. Am. Chem. Soc.*, 2013, **135**, 18866-18875.
38. Y. You, Z. Ni, T. Yu and Z. Shen, *Appl. Phys. Lett.*, 2008, **93**, 163112-163112-163113.